

# Afterglows from precursors in Gamma Ray Bursts. Application to the optical afterglow of GRB 091024

F. Nappo<sup>1,2\*</sup>, G. Ghisellini<sup>2</sup>, G. Ghirlanda<sup>2</sup>, A. Melandri<sup>2</sup>, L. Nava<sup>3</sup>, D. Burlon<sup>4</sup>

<sup>1</sup> *Università degli Studi dell'Insubria, via Valleggio 11, I-22100 Como, Italy*

<sup>2</sup> *INAF – Osservatorio Astronomico di Brera, Via Bianchi 46, I-23807 Merate, Italy*

<sup>3</sup> *Racah Institute for Physics, The Hebrew University of Jerusalem, 91904, Israel*

<sup>4</sup> *Sydney Institute for Astronomy, School of Physics, The University of Sydney, NSW 2006, Australia*

28 August 2019

## ABSTRACT

About 15% of Gamma Ray Bursts have precursors, i.e. emission episodes preceding the main event, whose spectral and temporal properties are similar to the main emission. We propose that precursors have their own fireball, producing afterglow emission due to the dissipation of the kinetic energy via external shock. In the time lapse between the precursor and the main event, we assume that the central engine is not completely turned off, but it continues to eject relativistic material at a smaller rate, whose emission is below the background level. The precursor fireball generates a first afterglow by the interaction with the external circumburst medium. Matter injected by the central engine during the “quasi-quiet” phase replenishes the external medium with material in relativistic motion. The fireball corresponding to the main prompt emission episode crashes with this moving material, producing a second afterglow, and finally catches up and merges with the first precursor fireball. We apply this new model to GRB 091024, an event with a precursor in the prompt light curve and two well defined bumps in the optical afterglow, obtaining an excellent agreement with the existing data.

**Key words:** gamma rays: bursts, radiation mechanisms: non-thermal, gamma rays: observations

## 1 INTRODUCTION

Around 15% of Gamma Ray Bursts (GRBs), show precursors in the light curve of their prompt emission. Despite its definition is somewhat subjective, a “precursor” can be identified as emission (i) preceding main event, with a maximum flux (or count rate) which is less than the main event, and (ii) separated from the latter by a time interval in which the flux is at the background level (for different definitions of precursors and different ways to find GRBs with precursors see Koshut et al. 1995, Lazzati 2005, Burlon et al. 2008, 2009).

The main question is whether precursors have a different origin than the main event in GRBs or not. This issue has been explored observationally by comparing the energetics and spectra of precursors with those of the main event and more in general with those of GRBs without precursors (e.g. Burlon et al. 2008, 2009). The spectrum and variability timescale of precursors are similar to those of the main event. On average, precursors have a fluence (flux integrated over its duration) about one tenth of that of their associated main events. Also the time evolution of the spectrum of

precursors is consistent with that of GRBs without precursors (Burlon et al. 2009). These facts strongly suggest that the precursors are not a separated emission component, produced by something different from the central engine responsible for the main event. They are simply the first phases of the central engine activity.

The key question is then why the central engine can have periods of time in which it is quiescent. Some GRBs showed more than one precursors, and precursors have been seen also in short bursts (a typical example is GRB 090510, a very bright short GRB observed also above 100 MeV by the Large Area Telescope onboard the *Fermi* satellite, see Ackermann et al. 2010; for other examples see Troja, Rosswog & Gehrels 2010).

The explanation of the precursor phenomenon has remained a puzzle. The fact that there can be more than one precursors in one GRB rules out the “two step engine” model (see e.g. Wang & Mészáros 2007; Lipunova et al. 2009) in which the precursor corresponds to the formation of a compact object that after a while collapses onto a black hole, originating the main GRB event. The fact that the spectrum is not a blackbody (Lazzati et al. 2005; Burlon et al. 2008, 2009) and that the quiescent times are often very long rule out the fireball precursor models (see e.g. Mészáros & Rees 2000; Ruffini et al. 2001; Daigne & Mochkovitch 2002; Lyutikov &

\* Email: francesco.nappo@brera.inaf.it

Blandford 2003; Li 2007) that associate the precursor emission to the thermal radiation initially trapped in the fireball. Analogously, the non-thermal nature of the precursor’s spectrum rules out the “progenitor precursor” models (Ramírez-Ruiz et al. 2002; Lazzati & Begelman 2005) based on the collapsar scenario, in which the precursor corresponds to the interaction of a weakly relativistic jet with the stellar envelope.

Recently, Bernardini et al. (2013, 2014) put forward a new model able to explain the presence of one or more precursors with non-thermal emission. They assume that the central powerhouse is a newly born accreting magnetar; in this model accretion can be halted by the centrifugal drag exerted by the rotating magnetosphere onto the infalling matter, allowing for multiple precursors and very long quiescent times.

So far, however, precursors have been studied only in relation to the fact that they are observed in the high energy prompt light curve of GRBs. Here we consider the possibility that some features of the afterglow emission can be ascribed to the precursor activity. Indeed, since the energy emitted by precursors is a large fraction (10–50%) of the total energy of the bursts, we can assume that precursors originate fireballs as well as it is thought for the main event, and that these fireballs run into the circumburst medium (CBM).

Therefore, precursors should produce an external shock, namely, an afterglow, similarly to what is thought to happen for the main emission episode of any GRB. When the quiescent time between the precursors and the main event is sufficiently long, as in the case of GRB 060124 (Romano et al. 2006) and GRB 050820A (Cenko et al. 2006), we have the opportunity to see this afterglow emission (in between the precursor and the main event episodes).

The precursor fireball, being the first to interact with the CBM, will “sweep” it and set it in motion with a certain velocity. Then the central engine enters a phase of quiescence, ejecting matter at a much reduced rate, whose emission remain below the background level. This matter populates the circumburst region. When the central engine becomes active again, producing the main event of the prompt emission, a new fireball is produced, running into the *moving* CBM ejected during the quiescence phase. The corresponding shock is weaker than the shock into a stationary CBM, since the relative kinetic energy between the shock and the moving CBM is less than in the case of an unperturbed and stationary CBM. The main event fireball would then decelerate less, and it will catch up the first fireball, shock it, and merge.

We apply these ideas to a specific burst, GRB 091024 (Gruber et al. 2011; Virgili et al. 2013), a very long bursts ( $T_{90} = 1024$  s) with a precursor lasting  $\sim 70$  seconds, a quiescent time of  $\sim 600$  seconds, a second precursor lasting  $\sim 40$  s, another quiescent time of  $\sim 170$  seconds, and a complex main event, lasting  $\sim 200$  seconds with pronounced variability.

The long duration and quiescent time allowed to have a dense optical coverage of the light-curve, especially during the quiescent time (Virgili et al. 2013). Its properties make GRB 091024 an ideal test case for our new scenario, and we anticipate that the results are very encouraging.

In §2 we describe the main features of the proposed scenario, we detail its dynamical and radiative evolution in §2.2, 2.3, 2.4. The model is then applied to the optical light curve of GRB 091024 in §3 and §4. We draw our conclusions in §4.

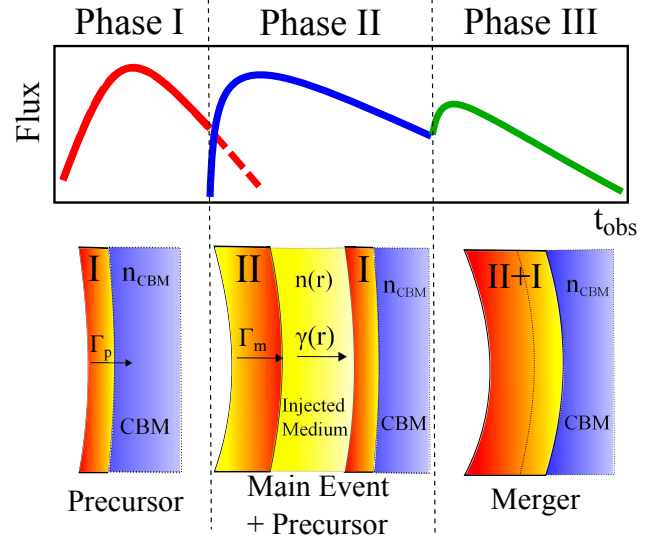


**Figure 1.** Cartoon of the proposed scenario. On the top we show the three phases of the afterglow emission, that correspond to the three configurations illustrated in the bottom: Phase 1): Fireball I (associated to the precursor) runs into the circumburst medium originating the first afterglow. Phase 2): Fireball II (associated to the main event) runs into the moving material ejected by the central engine during the quiescent phase, producing the second peak of the afterglow light curve. Phase III: Fireballs I and II merge, producing a brightening of the afterglow.

## 2 PROPOSED SCENARIO

Previous works (Burlon et al. 2008) showed that precursors have spectral and temporal properties similar to the main event emission, so it is reasonable to think that the same central engine is responsible for both. Fig. 1 shows a cartoon of the proposed scenario, whose main features can be summarized as follows:

- The precursor, being nothing else that the first pulse of the prompt emission, produces its own fireball (called “fireball I” hereafter) that shocks the circumburst material (with density  $n_{\text{CBM}}$ ) producing an afterglow emission (the peak is shown by the solid red line in the top panel of Fig.1).
- During the “quiescent” phase of apparent no emission, the central engine is not completely switched off, but that it continues to eject relativistic matter, albeit at a much reduced rate. At the end of this quiescent phase, the central engine fully reactivates, producing the main prompt event associated to “fireball II”.
- Fireball II can interact with this continuously ejected material and produce a second afterglow emission. The shock will be less efficient than the first one because it is produced in a medium that is moving. This explains the presence of a second peak in the optical light curve, in this case associated with the second emitted fireball, i.e. that of the main event.
- For simplicity, the density and the bulk Lorentz factor profile of the ejected medium are assumed to be power-laws:

$$\begin{aligned} n(r) &= n_0(r/r_0)^{-s} \\ \gamma(r) &= \gamma_0(r/r_0)^{-g} \end{aligned} \quad (1)$$

- If fireball I decelerates more than fireball II, by the interaction with the external medium, a merger between the two fireball occurs. During the merger some energy is released (with a mechanism that is similar to internal shocks) and a merged fireball (I+II) is formed. This fireball decelerates in the external medium generating the last part of the afterglow emission. This episode can be seen as an in-

jection of new kinetic energy from the fireball II to the decelerating fireball I (*refreshed shock*, Rees & Mészáros 1998). This produces a rebrightening episode.

Summarizing, we identify three distinct afterglow emission phases:

- (i) The first afterglow produced by the deceleration of fireball I in the CBM.
- (ii) The second afterglow produced by the deceleration of fireball II in the medium ejected by the central engine, albeit at a reduced rate;
- (iii) The last part of the afterglow produced by the merged fireballs (I+II) interaction with the external medium.

For each of these three portions we need to study the dynamical behaviour of the fireball and how the dissipated energy is converted into radiation.

## 2.1 Dynamics

The dynamical study, inspired by Nava et al. (2013), is based on the energy–momentum conservation in the collision of the fireball with the external CBM. In this case we must consider that the external medium can be pre-accelerated with a Lorentz factor profile  $\gamma(r)$ .

We assume that the fireball has initial mass  $M_0$  and initial Lorentz factor  $\Gamma_0$ . In the collision with the external CBM, the fireball collects the mass of the encountered CBM and when the collected mass is about  $M_0/\Gamma_0$  the fireball starts to decelerate, reducing its Lorentz factor  $\Gamma(r)$ . In the collision, some bulk kinetic energy is transformed in internal energy  $\epsilon'$  (as measured in the fireball comoving frame). A fraction of this internal energy (labeled as  $\epsilon'_{\text{RAD}}$ ) is radiated and no longer contributes to the inertia of the fireball; the amount of radiated energy depends on the specific radiative process and it will be analysed in the following section.

If  $\epsilon'_{\text{RAD}} \ll \epsilon'$ , the fireball is a very inefficient radiator, so the radiative losses are negligible and the dynamical evolution of the fireball can be described separately by the radiative emission behaviour. Since the total fireball energy is conserved, this case is called *adiabatic regime*.

In the opposite case, if  $\epsilon'_{\text{RAD}} \sim \epsilon'$ , almost all the internal energy is lost in radiation. Also in this case the fireball dynamical evolution can be treated separately by the radiative emission, and it is called *radiative regime*.

In the intermediate case, the dynamical evolution is strictly linked to the radiative behaviour, so both aspects have to be considered simultaneously. From the momentum-energy conservation relations in the collision of the fireball with a CBM spherical shell of thickness  $\Delta r$ , we can obtain the internal energy  $\Delta \epsilon$  produced in the collision. A fraction  $\epsilon_e$  of this internal energy is given to the CBM electrons, that can emit a part of it as radiation. We assume that we can write the radiated energy  $\Delta \epsilon'_{\text{RAD}}$  as:

$$\Delta \epsilon'_{\text{RAD}}(r) = \zeta(r) \epsilon_e \Delta \epsilon'(r) \quad (2)$$

where  $\zeta(r)$  is the fraction of electron energy that is radiated at  $r$  (this value depends on the radiative process and it will be calculated in §2.3). We obtain the comoving emitted bolometric luminosity:

$$L'_{\text{bol}} = \frac{\Delta \epsilon'_{\text{RAD}}}{\Delta t'} = \frac{\Delta \epsilon'_{\text{RAD}}}{\Delta r} \frac{\Delta r}{\Delta t_{\perp}} \frac{\Delta t_{\perp}}{\Delta t'} = \Gamma \beta c \frac{\Delta \epsilon'_{\text{RAD}}}{\Delta r} \quad (3)$$

where  $\Delta t_{\perp} = \Delta r/(\beta c)$  is the time interval corresponding to the distance  $\Delta r$  measured by an observer placed perpendicularly to the burst direction and  $\Delta t'$  is the same time measured by a comoving observer.

## 2.2 Times

The time interval  $\Delta t_{\text{obs}}$  corresponding to the distance  $\Delta r$  measured by an observer placed close to the axis of the burst can be written as:

$$\Delta t_{\text{obs}} = (1+z) \frac{1 - \beta \cos \theta}{\beta c} \Delta r \quad (4)$$

where  $z$  is the cosmological redshift and  $\theta$  is the angle between the line of sight and the burst axis.

The observed bolometric luminosity observed at time  $t_{\text{obs}}$  is constituted by the photons arriving to the detector at the time  $t_{\text{obs}}$ , but that have been emitted at different times. The real emitting surface seen at time  $t_{\text{obs}}$  is called *equal arrival time surface* and it is non-trivial to determine.

We approximate the determination of the equal arrival time surfaces by considering that most of the received emission comes from the ring of aperture angle  $\sin \theta = 1/\Gamma$  (or equivalently  $\cos \theta = \beta$ ). In this way Eq. 4 simplifies in

$$\Delta t_{\text{obs}} = (1+z) \frac{\Delta r}{\beta c \Gamma^2} \quad (5)$$

The observed bolometric luminosity can be written as:

$$L_{\text{bol}} = \delta^2 L'_{\text{bol}} \quad (6)$$

where  $\delta = [\Gamma(1 - \beta \cos \theta)]^{-1}$  (equal to  $\Gamma$  for  $\cos \theta = \beta$ ) is the relativistic Doppler factor (or beaming factor). The obtained bolometric luminosity is a function of time, so we will label it with  $L_{\text{bol}}(t)$ .

## 2.3 Radiative emission

In this section we calculate the synchrotron emission observed at the frequency  $\nu = \nu_{\text{obs}}(1+z)$ . We use an approach different from the one used by Panaitescu & Kumar (2000). The detailed description of the adopted method will be described elsewhere (Nappo et al., in prep.), here we mention the main points.

We explicitly apply an energy conservation equation, by requiring that in the fast cooling regime the frequency integrated spectrum is equal to the power that the shock gives to the electrons, as measured in the observer frame:

$$\int L_{\nu}(t) d\nu = \Gamma^2 \epsilon_e \frac{\Delta \epsilon'}{\Delta t'} \quad (7)$$

We assume that the synchrotron emission is produced by a distribution of electrons that is the result of a continuous particle injection and the cooling due to the emission. We label with  $Q(\gamma)$  the number of injected electrons with energy  $\gamma m_e c^2$  for unity of time and volume,  $N(\gamma)$  the energetic distribution for unity of volume and  $\dot{\gamma}$  the cooling rate. They are linked by the *continuity equation*:

$$\frac{\partial N(\gamma)}{\partial t} = \frac{\partial}{\partial \gamma} [\dot{\gamma} N(\gamma)] + Q(\gamma) \quad (8)$$

For a stationary source  $\partial N(\gamma)/\partial t = 0$ .

We assume that the injection distribution is a power law of index  $2 < p < 3$ :

$$Q(\gamma) \propto \gamma^{-p} \text{ for } \gamma_i < \gamma < \gamma_{\text{max}}, \quad (9)$$

where  $\gamma_i$  is called injection energy.

The synchrotron cooling rate is:

$$\dot{\gamma}_{\text{syn}} m_e c^2 = \frac{4}{3} \sigma_T c U_B \gamma^2 \quad (10)$$

The synchrotron cooling time is:

$$t_{c,\text{syn}} = \frac{\gamma}{\dot{\gamma}_{\text{syn}}} = \frac{3m_e c}{4\sigma_T U_B \gamma} \quad (11)$$

For each time, we define the cooling energy  $\gamma_c(t)m_e c^2$ , that is the energy that an electron must have so that its cooling time is equal to the scale time of expansion of the fireball. Under these conditions we have two possible solutions of Eq. 8:

a) *Fast Cooling regime*:  $\gamma_c < \gamma_i$ . In this case all injected electrons cool in a time shorter than the dynamical time (time needed to double the fireball radius). The corresponding energy distribution  $N_{\text{FC}}(\gamma)$  is

$$N_{\text{FC}}(\gamma) = \begin{cases} 0 & \gamma < \gamma_c, \\ N_i \left(\frac{\gamma}{\gamma_i}\right)^{-2} & \gamma_c < \gamma < \gamma_i, \\ N_i \left(\frac{\gamma}{\gamma_i}\right)^{-(p+1)} & \gamma_i < \gamma < \gamma_{\text{max}} \end{cases} \quad (12)$$

b) *Slow Cooling regime*:  $\gamma_i < \gamma_c$ . In this case a fraction of (or all) the injected electrons do not cool in a dynamical time. The corresponding energy distribution  $N_{\text{SC}}(\gamma)$  is

$$N_{\text{SC}}(\gamma) = \begin{cases} 0 & \gamma < \gamma_i, \\ N_c \left(\frac{\gamma}{\gamma_c}\right)^{-p} & \gamma_i < \gamma < \gamma_c, \\ N_c \left(\frac{\gamma}{\gamma_c}\right)^{-(p+1)} & \gamma_c < \gamma < \gamma_{\text{max}} \end{cases} \quad (13)$$

In this work we will not derive the normalizations  $N_i$  and  $N_c$  of the electrons energy distribution, but we will compute directly the normalizations of the emitted synchrotron spectrum (see §2.3.3).

### 2.3.1 Break frequencies

Generalizing Panaitescu & Kumar (2000) in the case of a pre-accelerated medium<sup>1</sup> we have the following relations:

$$\gamma_i = \epsilon_e \frac{m_p}{m_e} \frac{p-2}{p-1} (\Gamma_{\text{rel}} - 1) \quad (14)$$

$$\gamma_c = \frac{15\pi}{1+y} \frac{m_e c^2 \Gamma}{\sigma_T B^2 r} \quad (15)$$

$$U_B = \frac{B^2}{8\pi} = \epsilon_B n(r) m_p c^2 (\Gamma_{\text{rel}} - 1) (4\Gamma_{\text{rel}} + 3) \quad (16)$$

$$y = \frac{4}{3} \tau_e \langle \gamma^2 \rangle \quad (17)$$

$$\tau_e = \frac{1}{4\pi} \frac{\sigma_T m(r)}{m_p R^2} \quad (18)$$

where  $U_B$  is the magnetic energy density,  $y$  is the Comptonization parameter,  $\tau_e$  is the electron optical depth,  $\langle \gamma^2 \rangle$  is the average of the square of the random electron Lorentz factor,  $\Gamma_{\text{rel}}$  is the relative Lorentz factor between the fireball and the external medium, as measured in one of the two frames, and  $\epsilon_e$ ,  $\epsilon_B$  are the fractions of the dissipated internal energy that are given respectively to leptons and to the magnetic field.

The injection and the cooling frequency are:

$$\nu_i = \frac{4}{3} \frac{eB}{2\pi m_e c} \Gamma \gamma_i^2 \quad (19)$$

$$\nu_c = \frac{4}{3} \frac{eB}{2\pi m_e c} \Gamma \gamma_c^2 \quad (20)$$

For simplicity, we will not consider the self-absorbed part of the spectrum, since it is less relevant for the total energy and we are not interested to describe the radio light curve. The fraction of emitted energy  $\zeta$  (cfr. Eq. 2) can be expressed as the ratio between the power emitted in slow cooling regime and in fast cooling regime.

$$\zeta = \frac{[\int N(\gamma) \dot{\gamma} d\gamma]_{\text{SC}}}{[\int N(\gamma) \dot{\gamma} d\gamma]_{\text{FC}}} = \begin{cases} \frac{\gamma_i}{\gamma_c} \frac{p-2}{3-p} \left[ \frac{1}{p-2} \left( \frac{\gamma_c}{\gamma_i} \right)^{3-p} - 1 \right] & \gamma_i \leq \gamma_c, \\ 1 & \gamma_c < \gamma_i \end{cases} \quad (21)$$

where we used  $\dot{\gamma} = \dot{\gamma}_{\text{syn}}$ . Obviously, in the fast cooling regime we must have  $\zeta = 1$ .

### 2.3.2 Comptonization parameter $y$

We introduce here a new way to estimate the Comptonization parameter  $y$ . The bolometric luminosity is constituted by two main components: the synchrotron emission and the SSC.

$$L'_{\text{syn}} + L'_{\text{SSC}} = L'_{\text{bol}} = \zeta(y) P'_e \quad (22)$$

where  $P'_e$  is the total power distributed to the electrons, i.e. (cfr. Eq. 2):

$$P'_e = \epsilon_e \frac{\Delta \epsilon'}{\Delta t'} \quad (23)$$

$P'_e$  is obtained from purely dynamical considerations and does not depend on the particular emission mechanism chosen. We can express the synchrotron luminosity as (see Ghisellini et al. 2010):

$$L'_{\text{syn}} = \int 4\pi r^2 \Delta r' N(\gamma) \dot{\gamma}_{\text{syn}} m_e c^2 d\gamma \quad (24)$$

Following Eq. 17 we have

$$y = \frac{4}{3} \sigma_T \Delta r' \int N(\gamma) \gamma^2 d\gamma \quad (25)$$

The we have:

$$L'_{\text{syn}} = 4\pi R^2 c U_B y \quad (26)$$

Dividing both sides for  $4\pi r^2 c$  we obtain the energy density of the synchrotron emission:

$$U_{\text{syn}} = \frac{L'_{\text{syn}}}{4\pi R^2 c} = y U_B \quad (27)$$

Then we write the SSC luminosity as:

$$L'_{\text{SSC}} = 4\pi R^2 c U_{\text{syn}} y = y L'_{\text{syn}} = y^2 4\pi R^2 c U_B \quad (28)$$

valid as long as the scattering is in the Thomson regime. Combining the Eqs. 22, 26 and 28 we obtain an important relation:

$$4\pi R^2 c U_B (y + y^2) = \zeta(y) P'_e \quad (29)$$

We obtain the Comptonization parameter  $y$  by numerically solving:

$$\frac{y + y^2}{\zeta(y)} = \frac{P'_e}{4\pi R^2 c U_B} \quad (30)$$

<sup>1</sup> Note the different use of  $\Gamma$  and  $\Gamma_{\text{rel}}$

### 2.3.3 Normalized synchrotron spectrum

The synchrotron spectrum can be written as Eq. 31 or Eq. 32, in the fast and slow cooling regime respectively.

$$L_{\nu, \text{syn}}^{FC} = A_{FC} \begin{cases} \left(\frac{\nu}{\nu_c}\right)^{1/3} & \nu < \nu_c \\ \left(\frac{\nu}{\nu_c}\right)^{-1/2} & \nu_c < \nu < \nu_i \\ \left(\frac{\nu}{\nu_i}\right)^{-p/2} \left(\frac{\nu_c}{\nu_i}\right)^{1/2} & \nu_i < \nu < \nu_{\text{max}} \end{cases} \quad (31)$$

$$L_{\nu, \text{syn}}^{SC} = A_{SC} \begin{cases} \left(\frac{\nu}{\nu_i}\right)^{1/3} & \nu < \nu_i \\ \left(\frac{\nu}{\nu_i}\right)^{-(p-1)/2} & \nu_i < \nu < \nu_c \\ \left(\frac{\nu}{\nu_c}\right)^{-p/2} \left(\frac{\nu_i}{\nu_c}\right)^{(p-1)/2} & \nu_c < \nu < \nu_{\text{max}} \end{cases} \quad (32)$$

where  $A_{FC}$  and  $A_{SC}$  are normalizing constants. In Eqs. 31 and 32, we neglected the self-absorbed part of spectrum, because we do not consider the evolution of the radio afterglow. We can obtain the normalizations imposing:

$$L_{\text{syn}} + L_{\text{SSC}} = L_{\text{syn}}(1 + y) = L_{\text{bol}} \quad (33)$$

or

$$\int L_{\nu, \text{syn}} d\nu = \frac{L_{\text{bol}}}{1 + y} = \zeta \frac{\Gamma^2 \epsilon_e}{1 + y} \frac{\Delta \epsilon'}{\Delta t'} \quad (34)$$

where  $L_{\text{bol}}$  is obtained from the dynamical energy–momentum conservation. Remembering that  $\nu = \nu_{\text{obs}}(1 + z)$ , the observed monochromatic flux can be written as:

$$F_{\nu_{\text{obs}}} = \frac{\nu}{\nu_{\text{obs}}} \frac{L_{\nu}}{4\pi d_L^2} = (1 + z) \frac{L_{\nu}}{4\pi d_L^2} \quad (35)$$

where  $d_L$  is the luminosity distance. Determining for each time the specific flux  $F_{\nu_{\text{obs}}}$ , we obtain the monochromatic flux light curve, i.e. the function  $F_{\nu_{\text{obs}}}(t)$ .

With the above approach we obtain the monochromatic synchrotron light curves of the GRB afterglow in a way that ensures the conservation of energy and momentum.

## 2.4 Model parameters and observables

We can divide the model parameters in four groups.

### Precursor parameters

- $\Gamma_{0,p}$ : Initial Lorentz factor of the precursor fireball
- $E_{k,p}$ : Isotropic equivalent kinetic energy of the precursor fireball
- $T_p$ : Duration of the precursor emission
- $E_{\text{peak},p}$ : Peak energy of the precursor

The last two quantities are measurable and the kinetic energy  $E_{k,p}$  can be obtained by the isotropic equivalent energy of the precursor  $E_{\text{ISO},p}$  from the relation:  $E_{\text{ISO},p} = \eta E_{k,p}$ , where  $\eta$  is the efficiency of conversion of the kinetic energy in radiative energy. We will assume  $\eta \simeq 0.2$ . The isotropic equivalent energy can be obtained from the observed fluence  $\mathcal{F}$  with:

$$E_{\text{ISO}} = \frac{4\pi d_L^2}{(1 + z)} \mathcal{F} \quad (36)$$

So the only free parameter of the precursor is the initial Lorentz factor  $\Gamma_{0,p}$ . For simplicity, we assume that the circumburst medium where the precursor propagates is homogeneous, with density  $n_{\text{CBM}} = 3 \text{ cm}^{-3}$ .

### Main event parameters

- $\Gamma_{0,m}$ : Initial Lorentz factor of the main event fireball
- $E_{k,m}$ : Isotropic equivalent kinetic energy of the main event fireball
- $T_m$ : Duration of the main event emission
- $E_{\text{peak},m}$ : Peak energy of the spectrum of the main event
- $\Delta t_{\text{main}}$ : Start time of the main event emission after the trigger

$\Delta t_{\text{main}}$  can be directly observed. As in the previous case, the only free parameter is the initial Lorentz factor  $\Gamma_{0,m}$ .

### Injected medium parameters

The matter injected by the central engine in the quasi-quiescence phases can be described with 4 parameters characterizing the density  $n(r)$  and velocity  $\gamma(r)$  profile, i.e.  $\gamma_0$ ,  $g$ ,  $n_0$  and  $s$  (see Eq. 1).

### Merging parameters

These parameters describe the third phase of the afterglow light curve, after the merging of fireball I and II.

- $t_{\text{merg}}$ : Merging time of the two fireballs
- $\Gamma_{\text{merg}}$ : Initial Lorentz factor of the merged fireball
- $E_{k,\text{merg}}$ : Isotropic equivalent kinetic energy of the merged fireball

In this group there are no free parameters. The merging time  $t_{\text{merg}}$  can be determined studying the motion of the fireballs I and II that is completely determined from the parameters  $\Gamma_p(t)$ ,  $\Gamma_m(t)$ , and the medium properties.  $\Gamma_{\text{merg}}$  and  $E_{k,\text{merg}}$  can be obtained from the equation of energy–momentum conservation during the merging.

### Energy distribution parameters

For each part of the afterglow light curve, there are three free parameters:

- $\epsilon_e$ : Fraction of the internal energy given to electrons
- $\epsilon_B$ : Fraction of the internal energy given to magnetic field
- $p$ : Injection spectral index of the electrons

Obviously we must have  $\epsilon_e + \epsilon_B < 1$ .

The model has many free parameters (15), but they can be determined or limited by the observational data. The position of the peaks and the slopes in the light curves are the main observables that can constrain the parameters value. In particular we have:  $(t_p, F_{\nu,p})$  that are respectively the time and flux of the peak of the precursor afterglow,  $(t_m, F_{\nu,m})$  of the peak of the main event afterglow,  $(t_{\text{merg}}, F_{\nu,\text{merg}})$  that are the time and flux corresponding to the moment of the merger between fireball I and II.

From the slopes (especially for the second afterglow peak) we can infer the features of the central engine injected medium.

## 3 APPLICATION TO GRB 091024A

As an application of our model, we study the broad band emission of GRB 091024A, an extremely long GRB, with  $T_{90} \sim 1,020$  s with precursor and a double peaked optical light curve. This burst is particularly suited to test our proposed model also because its optical light curve is highly sampled from 100 s to 1 day after the prompt emission. It was first detected by Fermi/GBM, that triggered at 08:55:58.47 UT ( $t_0$ ) and again at 09:06:29.36 UT (Bissaldi & Connaughton, 2009). It was observed also by Konus-Wind (Golenetskii et al. 2009), and by *Swift*/BAT (Marshall et al.,

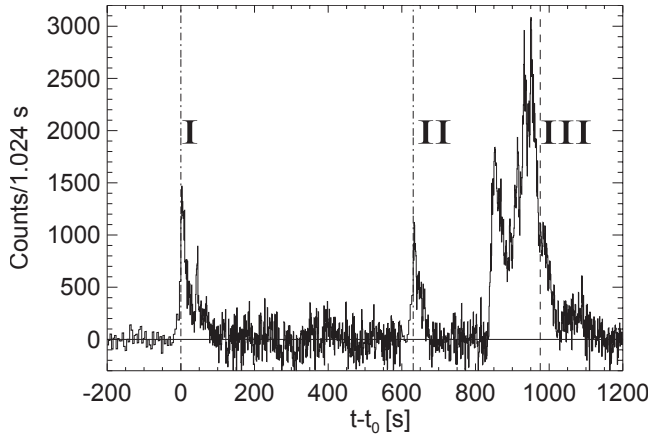


**Figure 2.** Prompt light curve of GRB 091024 background corrected in energy range 8–1000 keV (Gruber et al., 2011).

2009), but the burst exited the BAT field of view at  $t \sim 460$  s after the trigger and XRT measurements are available only  $\sim 3,000$  s after the GBM trigger, because of Earth–limb constraints. The burst coordinates, according to XRT, are  $\alpha_{J2000} = 22^h 37^m 00.4$ ,  $\delta_{J2000} = 56^\circ 53' 21''$ , with an accuracy of 6 arcsec (Page & Marshall, 2009). *Fermi*/LAT was re-pointed at the burst direction, but it did not reveal any significant emission (Bouvier et al., 2009).

The acquisition of the first optical data started about a minute after the first trigger by the Super-LOTIS telescope (Updike et al., 2009). Other photometric data come from the Sonoma Research Observatory (SRO) and the Faulkes telescopes. The afterglow optical spectrum was obtained with the Low Resolution Imaging Spectrometer on telescope Keck I and by the spectrograph GMOS-N on Gemini North, measuring a cosmological redshift of  $z = 1.092$  (Cenko et al., 2009; Cucchiara et al., 2009).

The optical data that we use for the physical interpretation of the afterglow are published in Virgili et al. (2013).

### 3.1 Prompt emission

The analysis of the entire prompt emission can be found in Virgili et al. (2013) and Gruber et al. (2011); here we present only the main results of these analyses and we focus on the afterglow emission interpretation. The background subtracted light curve of prompt emission measured by *Fermi*/GBM is shown in Fig. 2.

There are three emission episodes separated by two periods of quiescence or low activity. Because of the irregularity of the background level, from GBM data it is not possible to understand if there is a continuous activity of the central engine between the episodes or it is completely switched off. Instead, the Konus–Wind data show a low level emission in the period between the pulses (Virgili et al. 2013).

The main parameters obtained from the analysis of Gruber et al. (2011) and Virgili et al. (2013) are shown in Tab. 1. These parameters are obtained by fitting the prompt spectrum in each episode with a power–law with a high energy cut–off.

In the following section, we interpret the episodes I and II as emission due to the precursors and episode III as the main event, using the definition of precursor of Burlon et al. (2008).

### 3.2 Optical Afterglow

We study the optical afterglow in  $R'$  band (filter peak frequency  $\nu = 4.84 \times 10^{14}$  Hz.) The light curve is showed in Fig. 3.

There are two main peaks at  $t_{\text{obs}} \simeq 500$  s and  $t_{\text{obs}} \simeq 2,500$  s, and a small rebrightening at  $t_{\text{obs}} \simeq 5,000$  s. Fig. 3 shows also the flux multiplied by the observed time; in this representation, one sees at what time most of the flux is produced. It can be seen that the third peak is the most energetic one.

### 3.3 X–ray Afterglow

The X–ray emission of GRB 091024 has been observed by XRT only since about 3000 s after the trigger. We show the X–ray light curve here for completeness, although we do not pretend to reproduce it with our model. Indeed there are indications that the X–ray emission, particularly at early times after the GRB prompt emission, can be produced by a component which is not the standard afterglow (e.g. Ghisellini et al. 2006). This has been also shown recently with the study of the X–ray emission of a complete sample of GRBs detected by *Swift* (D’Avanzo et al. 2013). The XRT data (flux density at 1 keV) have been retrieved from the *Swift* Burst Analyzer. X–ray data are shown in Fig. 3.

### 3.4 Data Interpretation

To interpret the optical afterglow data, we applied this procedure dividing the light curve in three different time bins.

- (i)  $t_{\text{obs}} \lesssim 900$  s: Here the afterglow light curve is produced only by the interaction of the fireball of the precursor and the external medium (deceleration of fireball I).
- (ii)  $900 \text{ s} \lesssim t_{\text{obs}} \lesssim 5000$  s: The afterglow light curve is given by the superposition of the last part of the afterglow produced by the precursor (fireball I) and the one produced by the main event (fireball II).
- (iii)  $t_{\text{obs}} \gtrsim 5000$  s: Here the afterglow light curve is produced by the merger (fireball I+II) of the two fireballs.

We interpret the first peak as produced by the deceleration of fireball I, in the external homogeneous medium. The second peak is due to the deceleration of fireball II (main event) in the pre-accelerated medium injected by the central engine. The third peak corresponds with the merging of fireballs I and II. After the merging, the merged fireball I+II continues to decelerate in the external circumburst medium (that is not pre-accelerated), so it will produce a more intense and efficient emission. This medium jump causes a discontinuity in the light curve, alias the third peak. In this analysis we do not consider the second precursor (formerly labelled as Episode II). We have chosen to ignore Episode II for simplicity, since its energy is much smaller than the other two episodes (see also Tab. 1).

## 4 RESULTS

### 4.1 Optical Afterglow results

Fig. 3 shows the optical afterglow light curve compared with the model. There is a very good agreement between the model and the

Episode	$t - t_0$ [s]	$T_{90}$ [s]	$E_p$ keV	$\alpha$	$\mathcal{F}$ [ $10^{-5}$ erg/cm $^2$ ]	$E_{\text{ISO}}$ [ $10^{52}$ erg]
I	-3.8 : 67.8	$72.6 \pm 1.8$	$412_{-53}^{+69}$	$0.92 \pm 0.07$	$1.81 \pm 0.07$	$6.3 \pm 0.2$
II	622.7 : 664.7	$44.5 \pm 5.4$	$371_{-71}^{+111}$	$1.17 \pm 0.07$	$0.79 \pm 0.04$	$2.8 \pm 0.1$
III	838.8 : 1070.2	$150 \pm 10$	$278_{-18}^{+22}$	$1.38 \pm 0.02$	$6.73 \pm 0.09$	$23.6 \pm 0.3$

**Table 1.** Fit parameters of the three episodes of GRB 091024. The model fit is a cut-off power-law. Fluence between 8 keV and 40 MeV (Gruber et al., 2011).

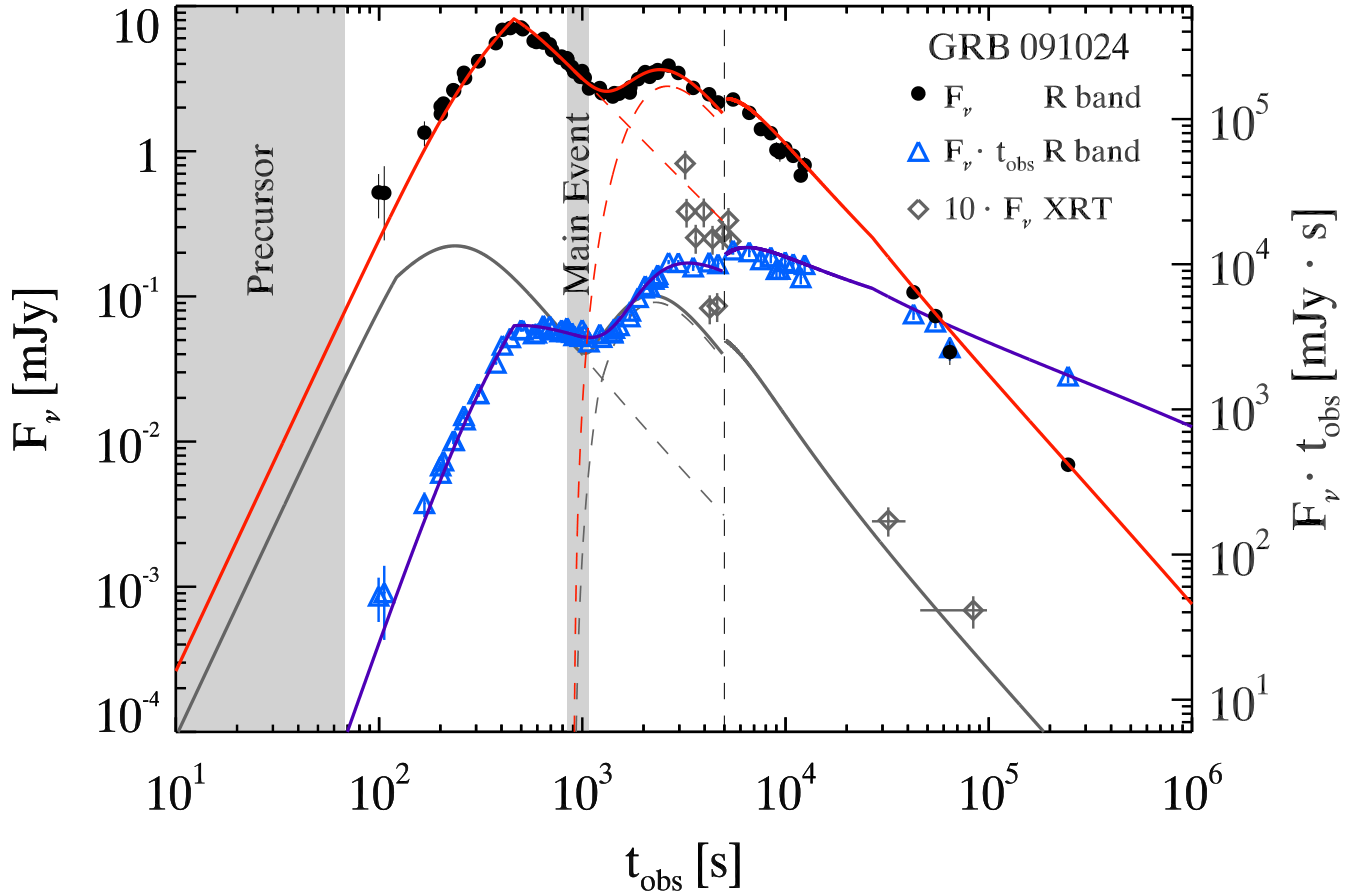


**Figure 3.** Afterglow light curve of the optical flux in mJy ( $R'$  band,  $\nu = 4.84 \times 10^{14}$  Hz, black dots) of GRB 091024 compared with the proposed model (red solid line). The afterglow emission of the precursor and the main event are shown by the red dashed lines. The vertical black dashed line represents the time when the two fireballs (of the precursor and of the main event) collide and merge in a new reborn fireball that decelerates in the external CBM. The blue triangles represent the monochromatic flux multiplied by the observed time, to better show when most of the flux has been emitted. The grey diamonds show the XRT X-ray emission at 1 keV multiplied by 10, compared with the prediction of the model for that frequency. The grey regions show the time of the precursor and the main event prompt emission.

data. The values of the parameters<sup>2</sup> used for the solution of the Fig. 3 are shown in Tab. 2 (fireballs parameters) and in Tab. 3 (medium parameters).

The connection between parameters and observables is not easy to make explicit, because each parameter affects several observables. It is therefore difficult to know, analytically, if the solution is unique. However, numerically, we have tried many combina-

Portion	$\Gamma_0$	$\Gamma_{\text{merg}}$	$\epsilon_e$	$\epsilon_B$	$p$
I	130	...	0.023	$6.0 \times 10^{-4}$	2.7
II	73	...	0.028	0.017	2.5
III	...	39.9	0.0045	0.003	2.6

**Table 2.** Model parameters for the three portions of the light curve: I) Precursor afterglow emission, II) Main Event afterglow emission, III) Afterglow emission produced after the merger of the precursor and the main event fireball.

<sup>2</sup> Consider that the value of  $\Gamma_0$  in the third portion is computed with the equation of momentum-energy conservation during the merger of the fireballs I and II and it is not a free parameter of the model.



$n_0$	$7.7 \times 10^7$	$\text{cm}^{-3}$
$s$	1	
$\gamma_0$	250	
$g$	0.25	

**Table 3.** Parameters of the medium injected by the central engine in the quasi-quietness phases (for  $r_0 = 10^{11}$  cm, see Eqs. 1).

tions of parameters, finding good fits only with values in a narrow range around the ones reported in Tabs. 2 and 3.

The values of the kinetic energy of the precursor and the main event have been computed from the prompt light curve (see Tab 1), assuming an efficiency  $\eta = 0.2$ , resulting in  $E_{k,p} \simeq 3 \times 10^{53}$  erg and  $E_{k,m} \simeq 1.3 \times 10^{54}$  erg<sup>3</sup>. Note that the ratio of the kinetic energy is comparable to the ratio of the energies that are emitted in each part of the afterglow (see also the flux multiplied by time Fig. 3).

#### 4.1.1 Precursor analysis

In this section we will focus on the solution for the optical light curve of the precursor.

At early times, we can see a growth of the flux with a slope steeper than  $t^2$ , becoming  $\propto t^2$  before the peak. The fast rising argues in favour of a homogeneous circumburst medium. Then there is a sharp peak followed by a flux decay steeper than  $t^{-1}$ . In Fig. 4 we show a detail of the optical light curve of the precursor afterglow, the break frequencies  $\nu_i$  and  $\nu_c$  and the Lorentz factor of the precursor fireball as a function of the observed time  $t_{\text{obs}}$ .

The observed peak is not due only to the deceleration of the fireball, but it is produced by the transition of the injection frequency  $\nu_i$ .

Moreover, we note that  $\nu_i < \nu_c$  always, so the afterglow emission of the precursor is always in the slow cooling regime.

#### 4.2 X-ray Afterglow results

We compare the XRT data sampling at 1 keV (Fig. 3, grey diamonds) and the light curve generated by the model at 1 keV, using the previous parameters obtained from the comparison with the optical afterglow light curve.

At early times the X-ray light curve is very irregular and shows a behaviour that is very different from the optical counterpart. We can interpret that emission as *late prompt* (Ghisellini et al. 2009), i.e. late central engine activity and not produced by the external shock of the decelerating fireball.

Conversely, the last two points show a decay of the X-ray flux that is consistent with the model predictions.

### 5 DISCUSSION

Since the general properties of precursors are very similar to the ones of the main events, it is natural to assume that precursors and main events are produced by the same central engine. The energetics of the precursors is less than, but close to, the energetics of

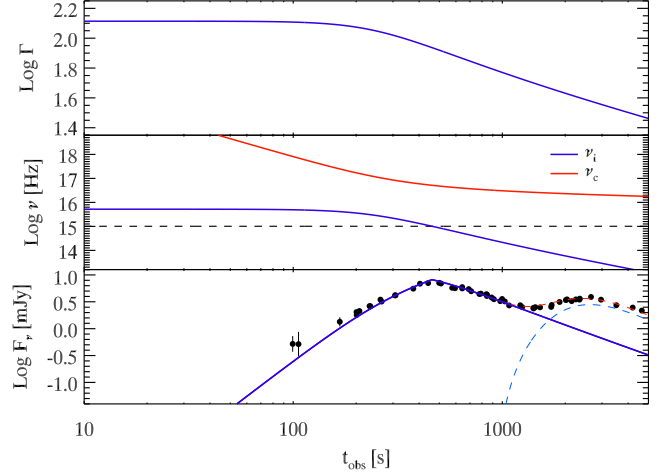


**Figure 4.** Afterglow emission from the precursor of GRB 091024. Top panel: Lorentz factor  $\Gamma$  as a function of the observed time  $t_{\text{obs}}$ . Center panel: the injection and cooling rest frame frequencies ( $\nu_i$  and  $\nu_c$  respectively) as a function of  $t_{\text{obs}}$ . The dashed line represents the rest frame frequency of observation ( $\nu = 1.01 \times 10^{15}$  Hz). All the frequencies are shown rest frame, i.e. corrected for the cosmological redshift. Bottom panel: optical ( $R'$  band) light curve of the afterglow emission of the precursor (solid line) resulting and main event light curve (dashed lines). We note that the afterglow peak corresponds at the passage of the injection frequency  $\nu_i$ .

the main event, and this implies that the precursor also generates its own fireball, that produces the first afterglow. As far as we know, this is the first time that the consequences of this scenario are explored. The onset of the first afterglow is linked to the energetics and the bulk Lorentz factor of the precursor, not the ones of the main event, and to the circumburst density. The main event launches a second, more powerful, fireball. It will run into a *moving* medium, producing afterglow emission not through a standard external forward shock, but with a less efficient kind of *internal* shock. The onset of this afterglow will then occur at a later time (the fireball takes longer to decelerate). The onset time will still depend on the energetics and the bulk Lorentz factor of the fireball, but in a different way than predicted by the standard theory. In addition, it will depend also on the density and velocity of the surrounding medium, ejected during the quiescent phase (i.e. the time interval between the precursor and the main event). Finally, when the second fireball reaches the first, we will have a third peak of the afterglow light curve. This can be considered as a refreshed shock. After the third peak, we have the standard behaviour.

We believe that this three-peak light curve is a distinguishing feature of the afterglow of the bursts with precursors in this idealized and simple case. There could be in fact a variety of cases: for instance, the burst could have more than one precursor (and this would increase the number of peaks in the light curve). Consider also that the second peak could not emerge, being hidden by the light curve produced by the first fireball (especially when the quiescent phase is short), or else the second fireball might not decelerate before catching the second fireball.

The proposed model well explain the optical afterglow of GRB 091024, which is otherwise difficult to understand (see the discussion in Virgili et al. 2013). Even if admittedly simplified (we have neglected the reverse shock and treated only the case of an homogeneous CBM), the model accounts for the observed optical light curve in a quite logical and simple way.

<sup>3</sup> In  $E_{k,m}$  is considered also the energy of the second precursor, previously called as “Episode II”.



## ACKNOWLEDGMENTS

We thank D. Gruber for discussion. PRIN–INAF 2011 is acknowledged for financial support.

## REFERENCES

- Ackermann M., Asano K., Atwood W.B., et al., 2010, *ApJ*, 716, 1178  
 Bernardini M.G., Campana S., Ghisellini G. et al., 2014, *MNRAS*, 439, L80  
 Bernardini M.G., Campana S., Ghisellini G. et al., 2013, *ApJ*, 775, 67  
 Bissaldi E. & Connaughton V., 2009, GCN circular N. 10070  
 Bouvier A., McEnery J., Chiang J., Kocevski D., Moretti E., Vasileiou V. & Piron F., 2009, GCN circular N. 10114  
 Burlon D., Ghirlanda G., Ghisellini G., Lazzati D., Nava L., Nardini M. & Celotti A. 2008, *ApJ*, 685, L19  
 Burlon D., Ghirlanda G., Ghisellini G., Greiner J. & Celotti A. 2009, *A&A*, 505, 569  
 Cenko S.B., Kasliwal M., Harrison F.A. et al., 2006, *ApJ*, 652, 490  
 Cenko S.B., Kasliwal M.M. & Kulkarni S.R., 2009, GCN circular N. 10093  
 Cucchiara A., Fox D. & Tanvir N., 2009, GCN circular N. 10065  
 Daigne F. & Mochkovitch R., 2002, *MNRAS*, 336, 1271  
 Ghisellini G., Ghirlanda G., Nava L. & Celotti A., 2010, *MNRAS*, 403, 926  
 Ghisellini G., Nardini M., Ghirlanda G. & Celotti A., 2009, *MNRAS*, 393, 253  
 Golenetskii R., Aptekar R., Mazets E., Palshin V., Frederiks D., Oleynik P., Ulanov M. & Svinkin D., 2009, GCN Circular N. 10083  
 Gruber D., Krhler T., Foley S., et al., 2011, *A&A*, 528, A15  
 Koshut T.M., Kouveliotou C., Paciesas W.S., et al., 1995, *ApJ*, 452, 145  
 Lazzati D., 2005, *MNRAS*, 357, 722  
 Lazzati D., & Begelman M.C., 2005, *ApJ*, 629, 903  
 Lipunova G.V., Gorbvskoy E. S., Bogomazov A.I., & Lipunov V.M., 2009, *MNRAS*, 397, 1695  
 Lyutikov, M., & Blandford, R. 2003 [arXiv:astro-ph/0312347]  
 Marshall F.E., Baumgartner W.H., Beardmore A.P. et al. 2009, GCN Circular N. 10062  
 Meszaros P., & Rees M. J. 2000, *ApJ*, 530, 292  
 Nava L., Sironi L., Ghisellini G., Celotti A., & Ghirlanda G., 2013, *MNRAS*, 433, 2107  
 Page K.L. & Marshall F.E., 2009, GCN circular N. 10069  
 Panaitescu A. & Kumar P., 2000, *ApJ*, 543, 66  
 Ramirez–Ruiz E., MacFadyen A.I., & Lazzati D. 2002, *MNRAS*, 331, 197  
 Rees M.J. & Meszaros P., 1998 *ApJ*, L496  
 Ruffini R., Bianco C.L., Frascchetti F., Xue S.–S., & Chardonnet P. 2001, *ApJ*, 555, L113  
 Troja E., Rosswog S. & Gehrels, N., 2010, *ApJ*, 723, 1711  
 Utdike A.C., Hartmann D.H., Milne P.A. & Williams G.G., 2009, GCN circular N. 10074  
 Virgili F.J., Mundell C.G., Pal’shin V. et al., 2013, *ApJ*, 778, 54  
 Wang, X.-Y., & Mészáros, P. 2007, *ApJ*, 670, 1247